Journal of Applied Electrochemistry (2007) 37:33–39
DOI 10.1007/s10800-006-9223-y

Modelling natural convection at complex surfaces and solid bodies using electrochemical techniques and flow visualisation

A.A. WRAGG[1] and J. KRÝSA[2,*]
[1]*Department of Engineering, University of Exeter, North Park Road, Exeter, EX4 4QF, UK*
[2]*Department of Inorganic Technology, Institute of Chemical Technology, Technická 5, l66 28, Prague 6, Czech Republic*
*(*author for correspondence, e-mail: josef.krysa@vscht.cz)*

Received 14 February 2006; accepted in revised form 28 March 2006

Key words: electrochemical technique, flow visualisation, heat transfer, mass transfer, natural convection

Abstract

Since the review by Wragg [Journal of Applied Electrochemistry, 21 (1991) 1047] of more than 15 years ago there has been a considerable research output involving the use of combined electrochemical and flow visualisation techniques to investigate complex flows in natural convection situations. This paper reviews recent work involving electrode geometries and orientations such as vertical cylindrical electrodes of varying aspect ratio, down pointing and up pointing pyramidal electrodes, down facing horizontal circular surfaces with different edge conditions, isosceles triangular surfaces of various inclinations, long narrow upward facing linear tracks, open upward facing cavity electrodes, upward and downward facing truncated cones, and inclined disks with either single or both sides active. This constitutes a wide range of experimentation in which new insights into data treatment and correlation have been obtained. We have used approaches taking account of the differing behaviours of the single sides of three dimensional objects and computing interference factors taking account of flow interactions. Some highly successful illustrations of data correlation for extremely complex situations are demonstrated. Flow visualisation for most of the above mentioned situations have been obtained using schlieren photography which has provided good illustrations of flow structure occurring at single faces of objects and in complexly interacting flows. In addition we have combined some flow visualisation sequences with monitoring of the current-time relationships at the onset of convection to illustrate flow development phenomena from the onset of convective instabilities to the achievement of steady state conditions.

1. Introduction

Since the review by Wragg [1] of more than 15 years ago there has been a considerable research output involving the use of combined electrochemical and flow visualisation techniques to investigate complex flows in natural convection situations. This type of work is pertinent to electrochemical processes in non-flowing liquids but also to the simulation of heat transfer problems in natural convection. In a number of practical and technological processes such as drying, control of surface temperature by evaporative cooling and the curing of material surfaces mass transfer with simultaneous heat transfer in free convection plays a dominant role. An important finding in this field is that a combined Grashof number can be used to account for thermal and concentration buoyancy forces [2].

Knowledge of free convective heat transfer and, therefore, the prediction of heat losses from various objects of complex geometry is very important [3] for instance in design for heat dissipation from electronic components [4]. Mass-transfer measurements are known to provide good simulation of free convective heat transfer [5]. The limiting diffusion current technique of mass-transfer measurement is attractive as a cold modelling method for heat transfer since the measurements are usually simpler, cheaper and speedier than direct heat transfer measurements. Moreover, it is also easy to determine the heat transfer performance of the individual surfaces in a complex multi-surface geometry.

To show the similarity between heat and mass transfer only the mass-transfer flux resulting from concentration gradients is considered in a non-reactive, two-component system. As an example, an electrochemical system in which species concentration differences at the electrodes occur is shown in Figure 1. This concentration gradient in the diffusion layer results in a density difference which causes a buoyancy force on the fluid close to the electrode surface within the existing body force field. If the diffusion layer is lighter than the ambient fluid the buoyancy force will cause an upward flow along the electrode.

This paper reviews recent work involving electrode geometries and orientations such as vertical cylindrical electrodes of varying aspect ratio [6], down-pointing and up-pointing pyramidal electrodes [7–9], down-facing hor-

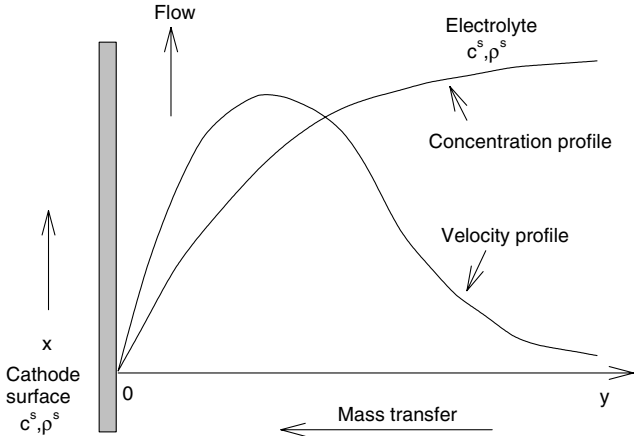

Fig. 1. Velocity and concentration distribution in natural convection flow along a vertical surface.

izontal circular surfaces with different edge conditions [10], isosceles triangular surfaces of various inclinations [11, 12], long narrow upward-facing linear tracks [13], open upward-facing cavity electrodes [14], down-pointing and up-pointing truncated cones [15, 16], and inclined discs with either single or both sides active [17]. This constitutes a wide range of experimentation in which new insights into data treatment and correlation have been obtained.

2. Mass-transfer measurement

Mass-transfer coefficients were calculated from measured limiting currents usually using the Cu deposition reaction in H_2SO_4. Depending on the surface exposed we can obtain mass-transfer coefficients for the individual surfaces, for combinations of surfaces and for the entire surface of solid bodies having complex geometry. An example of such an investigation is shown for the case of truncated cones in Figure 2 [16]. The superior mass-transfer performance of the up-facing horizontal base is immediately apparent, especially compared with the down-facing horizontal surface. The mass-transfer coefficient for the conical surface initially increases with height (from 0.2 to 1 cm) and then decreases.

The presence of the maximum can be explained as follows. The mass-transfer coefficient for vertical surfaces and inclined surfaces (constant inclination) decreases with increasing surface length because of the increase in diffusion layer thickness. But there is another effect which has to be taken into consideration – the effect of inclination angle. This produces an increase in the mass-transfer coefficient with increasing angle of inclination of the down-facing conical surface. Thus, in the case of constant top and bottom base diameters there are two opposed effects on the mass transfer at the conical surface; firstly the truncated cone height and secondly the inclination angle. The down-facing horizontal base exhibits low mass-transfer performance which decreases for truncated cones with heights of 0.5 and 0.2 cm, though the base diameter is constant. This can be explained by the effect of the isolated conical

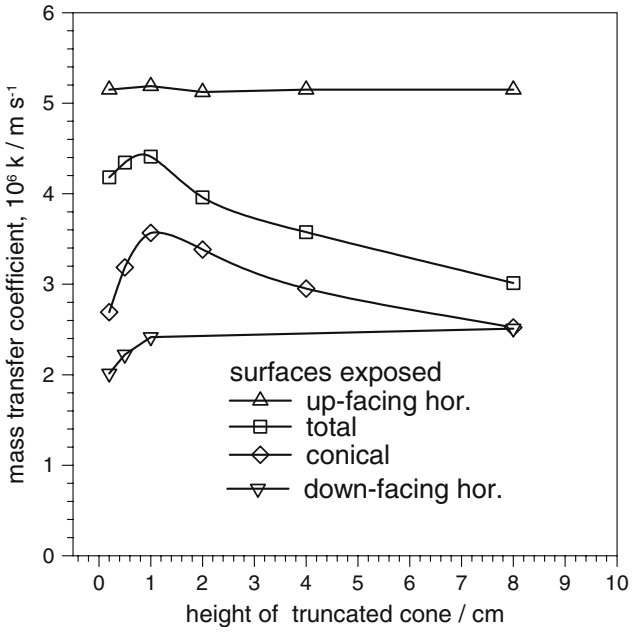

Fig. 2. Mass-transfer coefficient at individual surfaces of a down-facing truncated cone of constant top and bottom diameter.

surface adjacent to the horizontal base. These have inclinations progressively approaching the horizontal e.g. − 63° and − 79°, respectively. Thus the behaviour of the down-facing conical surface approaches that of a coplanar collared surface which has been shown [10] to have inferior mass-transfer performance to that of a surface with free edges. The mass-transfer coefficient for the entire surface broadly follows the same behaviour as for the conical surface alone. However, the values are increased by the superior behaviour of the up-facing horizontal base. The increase is especially apparent for truncated cones of heights from 0.2 to 1.0 cm. As for the conical surface alone, the entire truncated cone of 1 cm height shows the highest mass-transfer behaviour.

It is interesting to compare the mass-transfer coefficients for total truncated cones of constant top and bottom diameter and different orientation (Figure 3). For the lowest cone height (2 mm) the values are almost the same for both orientations. The reason is that a truncated cone approaches, for very small heights, a double-sided disc, so the effect of orientation is diminished. We can further see that for all heights greater than 2 mm, the down-pointing orientation exhibits better mass transfer performance, although it contains a down-facing conical surface. The down-facing conical surface exhibits lower mass-transfer rate than the up-facing conical surface (see Figure 2). But for total mass transfer the ratio of the up-facing and down-facing horizontal surfaces is of crucial importance.

3. Overall mass-transfer correlation

3.1. *Approach using Weber characteristic dimension*

Sometimes it is possible with such complex geometries to treat data using relatively simple "equivalent length"

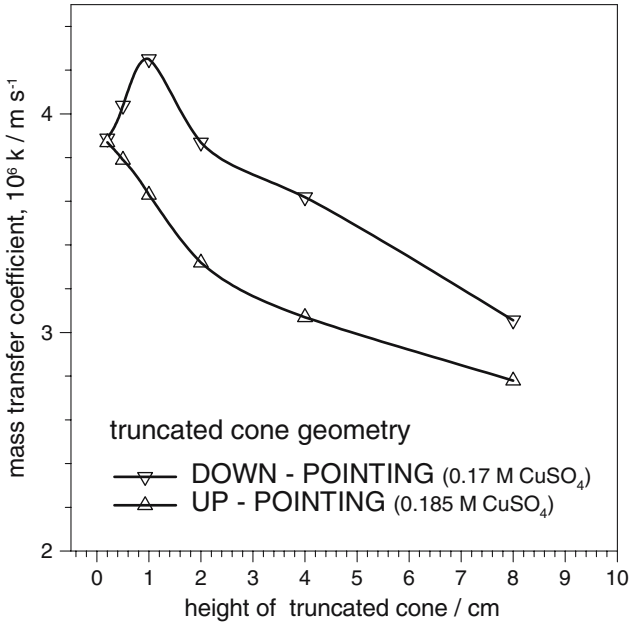

Fig. 3. Mass-transfer coefficient at a total truncated cone of constant top and bottom diameter; effect of orientation.

terms. The most often used single characteristic dimension which takes into account the relevant dimensions of a three-dimensional object was firstly introduced by Weber et al. [18] and is defined by Equation (1).

$$L_w = \frac{\text{surface area}}{\text{perimeter projected onto horizontal plane}} \quad (1)$$

A Rayleigh number and a Sherwood number based on this characteristic length L_w can then be defined.

$$\mathrm{Ra}_{L_w} = \mathrm{Gr}_{L_w}\mathrm{Sc} = \frac{g\Delta\rho L_w^3\rho}{\mu^2}\frac{\mu}{\rho D} \quad (2)$$

$$\mathrm{Sh}_{L_w} = \frac{kL_w}{D} \quad (3)$$

In our work the diffusivity of the Cu^{2+} ions was calculated using the data of Wilke et al. [19]. Electrolyte density and viscosity were calculated using data of Eisenberg et al. [20]. The $\Delta\rho$ terms were taken from [19]. The effect of migration on the copper deposition rate was negligible [21].

Such an approach was found to be successful in the case of vertical cavities with various height/diameter ratios (0.22–2.8) [14] where we found the correlation

$$\mathrm{Sh}_{L_w} = 0.559\mathrm{Ra}_{L_w}^{0.265} \quad (4)$$

for Ra_{L_w} in the range 2×10^7 to 1.2×10^{10} and Sc in the range 2050–2300. Furthermore re-evaluation of previous experimental data of Somerscales and Kassemi [22] also gave excellent agreement with this equation. This approach was also successful for the correlation of mass-transfer data from entire up-pointing truncated cones [15].

Frequently this simplification is inadequate in describing the complexities of interaction of flow streams originating from different surfaces of a solid body and then interacting. An example of such behaviour is a down-pointing truncated cone. The mass transfer data from entire down-pointing truncated cones are plotted in terms of Sherwood number vs. Raleigh number in Figure 4 using the characteristic length, L_w. It is seen that the data from the shorter truncated cones lie under the Weber correlation and the equation is entirely unsuited to the overall correlation of free convective mass transfer. This can be explained by the presence of the combination of a down-facing horizontal surface and a down-facing conical surface which is responsible for the low mass transfer, especially for low cone heights. Discrepancy with the Weber approach was also found when correlating natural convective mass transfer to cuboids [4], vertical cylinders with active ends [6] and down-pointing and up-pointing pyramids [7, 8]. We have therefore resorted to using approaches taking account of the differing behaviours of the single sides of three-dimensional objects and computing interference factors which take account of flow interactions.

3.2. *Summation approach to correlation for entire three-dimensional objects*

By summing the mass-transfer rates from correlations for the separate sides of an object a total mass-transfer

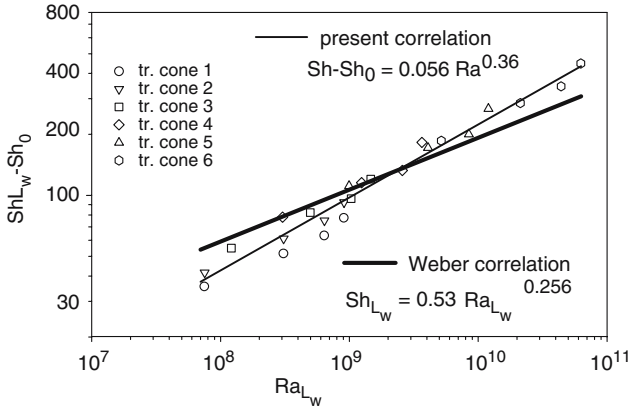

Fig. 4. Correlation of total mass-transfer data from down-pointing truncated cones using the Weber characteristic dimension.

performance can be predicted. An example of such treatment is shown here for down-pointing truncated cones.

The mass-transfer rates for separate surfaces were correlated using conical surface length (L) and the horizontal truncated cone base diameter (d) as characteristic lengths. The mass transfer from the whole surface comprises mass transfer from the down-facing horizontal base, the conical surface and the up-facing horizontal base:

$$\mathrm{Sh_t}A_\mathrm{t} = \mathrm{Sh_{hd}}A_\mathrm{hd} + \mathrm{Sh_c}A_\mathrm{c} + \mathrm{Sh_{hu}}A_\mathrm{hu} \tag{5}$$

where $\mathrm{Sh_{hd}}$, $\mathrm{Sh_c}$ and $\mathrm{Sh_{hu}}$ are Sherwood number for down-facing horizontal base, conical surface and up-facing horizontal base, respectively. Introducing correlations for single surfaces into Equation (5), evaluating total (A_t) and separate surface areas ($A_\mathrm{hd} = \pi d_2^2/4$, $A_\mathrm{c} = (d_1 + d_2)\pi L/2$ and $A_\mathrm{hu} = \pi d_1^2/4$) and rearranging we obtain the resultant predicted natural convection mass-transfer rate for down-pointing truncated cones

$$\mathrm{Sh}_L - \mathrm{Sh}_0 = \frac{\left[0.64(d_2)^2\mathrm{Ra}_L^{-0.03} + 1.36(d_1+d_2)\sqrt{L^2 - \frac{1}{4}(d_1-d_2)^2} + 0.18(d_1)^2\mathrm{Ra}_L^{1/12}\right]}{(d_1)^2 + (d_2)^2 + 2(d_1+d_2)L}\mathrm{Ra}_L^{0.25} \tag{6}$$

The behaviour predicted by Equation (6) was compared with the mass-transfer data for truncated cones. It was found in every case that the predicted rate was about 5–25% higher than the actual. The flow of the fluid around the down-facing horizontal base means that the conical and up-facing horizontal surfaces are exposed to solution which has already been depleted of cupric ions. This boundary layer spillover effect causes the overall mass transfer for a truncated cone to be lower than that for the equivalent summed separate surfaces. A multiplying factor, f (an interference factor), may be introduced to Equation (6) to represent the lower rate of mass transfer at the vertical and up-facing horizontal surfaces. Equation (6) now becomes:

$$\mathrm{Sh}_L - \mathrm{Sh}_0 = \frac{\left[0.64(d_2)^2\mathrm{Ra}_L^{-0.03} + f\left(1.36(d_1+d_2)\sqrt{L^2 - \frac{1}{4}(d_1-d_2)^2} + 0.18(d_1)^2\mathrm{Ra}_L^{1/12}\right)\right]}{(d_1)^2 + (d_2)^2 + 2(d_1+d_2)L}\mathrm{Ra}_L^{0.25} \tag{7}$$

where L is the conical surface length and d_1 and d_2 are the top and bottom horizontal diameters respectively and Ra_L is a Rayleigh number based on the conical surface length.

The applicability of correlating Equation (7) was tested for a set of truncated cones of different L/d_1 ratio. The values of f were obtained for each truncated cone from Equation (7). Sh_L–Sh_0 has been plotted to show the data from truncated cones of constant top to bottom diameter ratio against $\Phi(L,d_1,d_2, \mathrm{Ra}_L)\,\mathrm{Ra}_L$ in Figure 5. Here $\Phi(L,d_1,d_2, \mathrm{Ra}_L)$ is given by

$$\Phi(L,d_1,d_2,\mathrm{Ra}_L) = \left[\frac{0.64(d_2)^2\mathrm{Ra}_L^{-0.03} + f\left(1.36(d_1+d_2)\sqrt{L^2 - \frac{1}{4}(d_1-d_2)^2} + 0.18(d_1)^2\mathrm{Ra}_L^{1/12}\right)}{(d_1)^2 + (d_2)^2 + 2(d_1+d_2)L}\right]^4 \tag{8}$$

It can be seen that the data from truncated cones fit the line representing Equation (7) well and the fit is far better than that of the Weber correlation based on a single characteristic length.

The summation approach was applied to other objects such as down-facing and up-facing pyramids [7, 8] and vertical cylinders with active ends [6]. Similarly as for down-pointing truncated cones it was found that the mass-transfer rate for the combination of all inclined faces was lower than that for the single inclined surface. The interference factor (lower than 1) takes into account the fact that some surfaces of three-dimensional objects are exposed to fluid which has already been depleted in copper ions as it flows upward from the base. The dependence of the interference factor on the aspect ratio of the vertical cylinders (L/d), truncated cones (L/d_1), and down- and up-pointing pyramid (L/b) is shown in Figure 6. L is either the cylindrical, conical or inclined length, d and d_1 is the diameter of the cylinder or top base of the truncated cone, respectively, and b is side of the pyramid base. A schematic side view of four objects is shown in Figure 7. The dependence is very similar for cylinders and up-pointing pyramids where the interference factor increases with aspect ratio. This is caused by

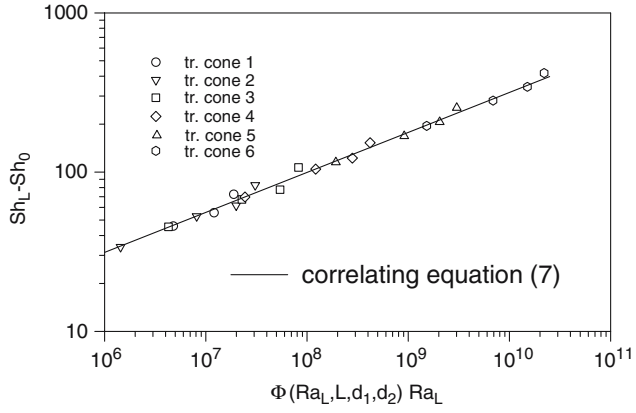

Fig. 5. Overall correlation for entire down-pointing truncated cones in terms of Equation (7).

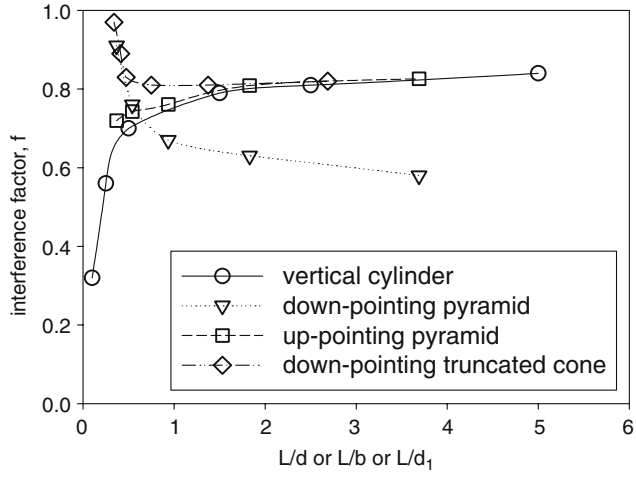

Fig. 6. Interference factor f as a function of aspect ratio.

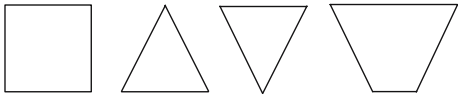

Fig. 7. Schematic side view of four three-dimensional objects. (A) vertical cylinder; (B) up-pointing pyramid; (C) down-pointing pyramid; and (D) down-pointing truncated cone.

the fact that the length of the surface exposed to fluid which has already been depleted in cupric ions increases while the size of the horizontal down-facing surface is constant. This means that the effect of cupric ion depletion, and thus the side interference, is much stronger for shorter vertical (inclined) lengths. On the other hand, for down-pointing pyramids, the interference factor f decreases with aspect ratio. This can be explained by the fact that the size of the up-facing horizontal base is constant and is exposed to fluid which has been increasingly depleted in cupric ions. This means that the effect of interference increases as inclined length increases.

Both these reasons for the behaviour of interference factor are mixed in the case of down-pointing truncated cones. For small cone heights where the difference between down-facing horizontal and down-facing inclined surfaces is very small due to the large inclination angle, similar behaviour to that for a down-pointing pyramid is observed. With increasing height the geometry of a truncated cone becomes more similar to that of a vertical cylinder and this results in the observed dependence of the interference factor.

4. Flow visualisation

Flow visualisation for most of the above-mentioned situations has been obtained using Schlieren photography which has provided some fascinating illustrations of flow structure occurring at single faces of objects and in complexly interacting flows. In addition, we have combined some flow visualisation sequences with monitoring of the current–time relationships at the onset of convection to illustrate flow development phenomena from the onset of convective instabilities to the achievement of steady-state conditions.

Vertical cavities, down-facing truncated cones and double-sided discs have been studied by this technique. As a first example photographs and transients for a down-facing truncated cone with height 0. 2 cm are shown in Figure 8. The transient is seen to undershoot and then overshoot the eventual steady convective limiting current, a behaviour similar to that observed for up-facing horizontal discs by Patrick and Wragg [23]. Flow begins as a ring of fluid rising from the upper cone periphery. It is notable that convection from the up-facing horizontal base is distinctly visible before the undershoot minimum is reached at about (t_m = 16 s). The sharp increase in the mass-transfer rate is then caused by the first main generation of convection streams from the up-pointing top which is well established at t = 35 s. Necking of the plume then occurs and a steady-state situation arises (t = 92 s) in which there is a complex flow structure consisting of a multiplicity of close-spaced interacting convection streams; the limiting current is seen to be very steady.

The second example is represented by cylindrical cavities of various inclinations. The photographs and transient for a vertical cavity of depth 0.65 cm were presented in [14] (as Figure 7). Flow begins as a ring of fluid emerging around the cavity diameter and is followed by a progressive necking of the resultant cylindrical plume. This then gives way to a single stream about 0.5 cm in diameter and, after about 50 s, some weak pulsation occurs. This demonstrates that the mass-transfer rate fluctuates in a regular fashion similar to the behaviour for upward facing horizontal discs [23]. As in the case of a truncated cone, the undershoot and overshoot in the current transients immediately following the early pure diffusional region, are also apparent. The undershoot and overshoot become less pronounced with increasing cavity depth and is not visible for

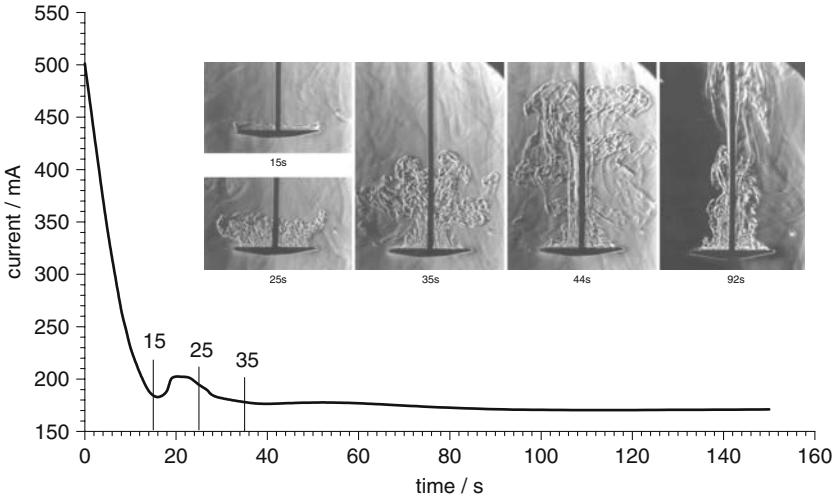

Fig. 8. Current transient and flow development for down-pointing truncated cone with height 2 mm (in 0.16 M copper sulfate).

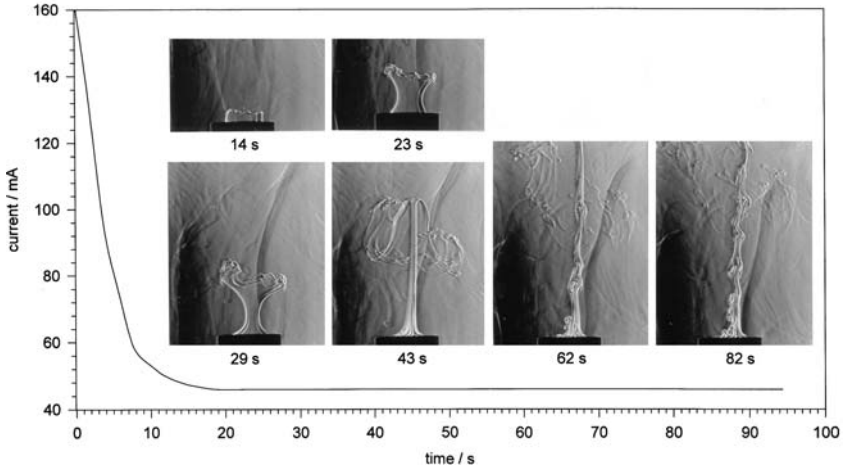

Fig. 9. Current transient and flow development for vertical cavity with inactive base and depth 0.99 cm (in 0.16 M copper sulfate).

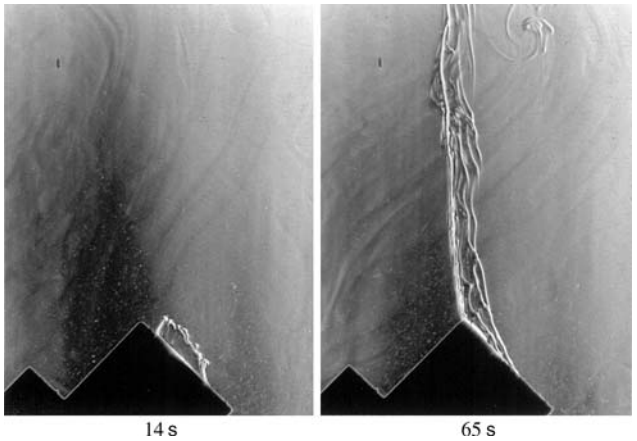

Fig. 10. Photographs of flow for total cavity of depth 0.99 cm inclined at 45° (in 0.16 M copper sulfate) at two different times following current onset.

cavities of depth greater than 1.6 cm because of the dominant behaviour of the cavity wall, resulting in the longer build up of the diffusion layer.

Photographs and a current transient for a cavity with inactive base (depth 0.99 cm) are shown in Figure 9. There was little difference between the observed flow regime for this cavity compared with the fully active one [14] except that the early stages of the plume appear less disturbed. Also, due to the base being inactive, the current–time transients do not exhibit the undershoot and overshoot typical of horizontal surfaces.

Photographs of flow from the 0.99 deep cavity inclined at 45° are shown in Figure 10 (0.16 M) at two different times. The inclined cavities all showed similar flow regimes with no pulsing observed. Figure 10 suggests that flow remains predominantly attached to the cavity walls prior to exit from the cavity mouth. When the cavity is horizontal the emergent flow formed a single continuous stream as shown in Figure 11. The

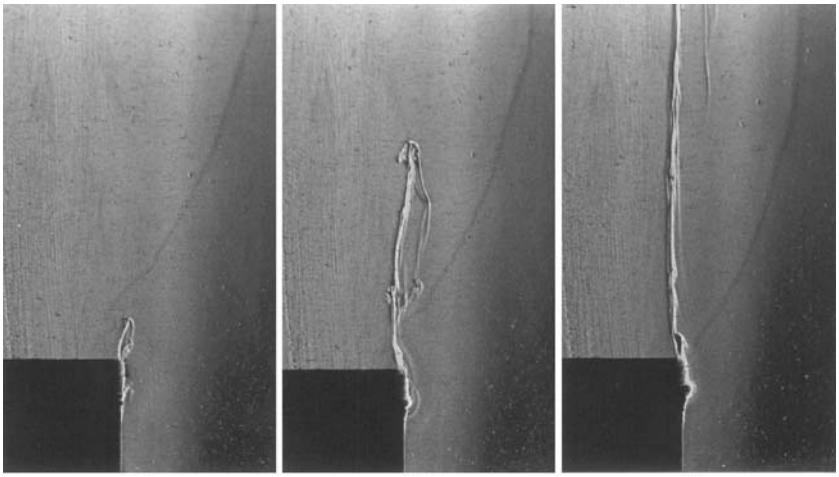

Fig. 11. Photographs of flow for total horizontal cavity of depth 1.21 cm (in 0.16 M copper sulfate) at three different times following current onset.

current transients for inclined and horizontal cavities did not show the degree of instability associated with pulsing observed in the case of some vertical cavities, this being consistent with the fact that only very weak flow pulsing was visually evident.

Acknowledgement

This study was partly supported by the Ministry of Education, Youth and Sports of the Czech Republic (project number MSM 6046137301).

References

1. A.A. Wragg, *J. Appl. Electrochem.* **21** (1991) 1047.
2. H. Sarac, A.A. Wragg and M.A. Patrick, *Int. Commun. Heat Mass Transfer* **18** (1991) 853.
3. W.M. Lewandovski, J.M. Khubeiz, P. Kubski, T. Wilczewski and S. Szymanski, *Int. J. Heat Mass Transfer* **41** (1998) 1857.
4. D.R.E. Worthington, M.A. Patrick and A.A. Wragg, *Chem. Eng. Res. Des.* **65** (1987) 131.
5. M.A. Patrick and A.A. Wragg, *I. Chem. Eng. Symp. Ser.* **94** (1985) 45.
6. J. Krýsa and A.A. Wragg, *J. Appl. Electrochem.* **22** (1992) 429.
7. J. Krýsa and A.A. Wragg, *Int. J. Heat Mass Transfer* **39** (1996) 1297.
8. J. Krýsa and A.A. Wragg, *Int. J. Heat Mass Transfer* **40** (1997) 3717.
9. J. Krýsa, F. Iino and A.A. Wragg, *Int. J. Heat Mass Transfer* **42** (1999) 3545.
10. A.A. Wragg, G. Batting and J. Krýsa, *Int. Commun. Heat Mass Transfer* **25** (1998) 175.
11. J. Krýsa, F. Iino and A.A. Wragg, *Collect. Czech. Chem. Commun.* **63** (1998) 2114.
12. M. Keppert, J. Krýsa and A.A. Wragg, *Collect. Czech. Chem. Commun.* **68** (2003) 2080.
13. C. Duchanoy, F. Lapicque, C.F. Oduoza and A.A. Wragg, *Electrochim. Acta* **46** (2000) 433.
14. J. Krýsa, A.A. Wragg, D.M. Thomas and M.A. Patrick, *Chem. Eng. J.* **79** (2000) 179.
15. J. Krýsa, A.A. Wragg and M.A. Patrick, *Int. J. Heat Fluid Flow* **23** (2002) 96.
16. J. Krýsa, D. Houf, C.F. Oduoza and A.A. Wragg, *Chem. Eng. J.* **85** (2002) 147.
17. J. Krýsa, W. Reuter and A.A. Wragg, *Int. J. Heat Mass Transfer* **48** (2005) 2323.
18. M.E. Weber, P. Austraukas and S. Petsalis, *Can. J. Chem. Eng.* **62** (1984) 68.
19. C.R. Wilke, C.W. Tobias and M. Eisenberg, *J. Electrochem. Soc.* **100** (1953) 513.
20. M. Eisenberg, C.W. Tobias and C.R. Wilke, *J. Electrochem. Soc.* **103** (1956) 413.
21. N. Ibl and O. Dossenbach. *in* E. Yeager, J.O.M. Bockris, B.E. Conway and S. Sarangapani (eds), Comprehensive Treatise of Electrochemistry 6, (Plenum Press, New York, 1983), pp. 192.
22. E.F.C. Somerscales and M. Kassemi, *J. Appl. Electrochem.* **15** (1985) 405.
23. M.A. Patrick and A.A. Wragg, *Int. J. Heat Mass Transfer* **18** (1975) 1397.